An interatomic potential model for molecular dynamics simulation of silicon etching by Br(+)-containing plasmas

AUTHOR(S):

Ohta, H.; Iwakawa, A.; Eriguchi, K.; Ono, K.

AIP Journal of Applied Physics

An interatomic potential model for molecular dynamics simulation of silicon etching by Br + -containing plasmas

H. Ohta, A. Iwakawa, K. Eriguchi, and K. Ono

Citation: Journal of Applied Physics **104**, 073302 (2008); doi: 10.1063/1.2990070
View online: http://dx.doi.org/10.1063/1.2990070
View Table of Contents: http://scitation.aip.org/content/aip/journal/jap/104/7?ver=pdfcov
Published by the AIP Publishing

JOURNAL OF APPLIED PHYSICS **104**, 073302 (2008)

An interatomic potential model for molecular dynamics simulation of silicon etching by Br^+-containing plasmas

H. Ohta,[a] A. Iwakawa, K. Eriguchi, and K. Ono
Department of Aeronautics and Astronautics, Graduate School of Engineering, Kyoto University, Yoshida-Honmachi, Sakyo-ku, Kyoto 606-8501, Japan

(Received 29 May 2008; accepted 12 August 2008; published online 6 October 2008)

An interatomic potential model for Si–Br systems has been developed for performing classical molecular dynamics (MD) simulations. This model enables us to simulate atomic-scale reaction dynamics during Si etching processes by Br^+-containing plasmas such as HBr and Br_2 plasmas, which are frequently utilized in state-of-the-art techniques for the fabrication of semiconductor devices. Our potential form is based on the well-known Stillinger–Weber potential function, and the model parameters were systematically determined from a database of potential energies obtained from *ab initio* quantum-chemical calculations using GAUSSIAN03. For parameter fitting, we propose an improved *linear* scheme that does not require any complicated nonlinear fitting as that in previous studies [H. Ohta and S. Hamaguchi, J. Chem. Phys. **115**, 6679 (2001)]. In this paper, we present the potential derivation and simulation results of bombardment of a Si(100) surface using a monoenergetic Br^+ beam. © *2008 American Institute of Physics*. [DOI: 10.1063/1.2990070]

I. INTRODUCTION

Understanding the interaction between chemical plasmas and material surfaces is of utmost importance when fabricating semiconductor devices. Recently, process sizes of device structures in the large-scale integration chips have reached a deep submicron level less than 50 nm. Therefore, a thorough (i.e., at the atomic-scale level) understanding via numerical simulations is necessary.

During plasma processing, high-energy ions (typically 10–500 eV) accelerated in the plasma sheath are injected into the material surface. In this case, a very large number of simulation particles are required for the dynamic simulation of reaction processes. Therefore, classical molecular dynamics (MD) simulation using a preconstructed interatomic potential model is very useful because the low simulation cost involved facilitates a systematic parameter survey.

The construction of a potential model is vital for performing classical MD simulations. Herein, we summarize the potential models developed for plasma etching simulations. Stillinger and Weber (SW) developed a potential model with two-body and three-body functions for Si and F systems.[1,2] These potential functions are designed to reproduce some of the structural and thermodynamic characteristics of the materials and the relevant structural chemistry for some selected molecules comprising these elements. Feil *et al.*[3] also applied this function form to Si and Cl systems by determining new parameter sets. Weakliem *et al.*[4] have modified the original SW potentials for Si–F systems using the interatomic potential data obtained from *ab initio* quantum-chemical calculations for performing MD simulations of fluorine adsorption on silicon. Hanson *et al.*[5] have also modified Feil's model for Si–Cl systems by adding new terms, i.e., an embedding term and a four-body term based on the *ab initio* data, in order to represent a highly realistic surface reaction during plasma etching including low-energy neutral radicals. Ohta *et al.*[6] developed two sets of potential models for Si–O–F and Si–O–Cl systems based on previously reported potential models for Si–F, Si–Cl, and Si–O systems with additional *ab initio* data. Here, the models for Si–O systems were originally developed by Watanabe *et al.*[7] for a large-scale modeling of SiO_2/Si interface structures. Further, a potential model with multibody interactions based on *bond-order* potential was developed by Tersoff,[8–10] and the parameters for Si, C, and Si–C systems have been currently made accessible. These potential models were extended to C–H systems by Brenner[11,12] in order to study various small hydrocarbon molecules as well as graphite and diamond lattices. Tanaka *et al.*[13] and Abrams *et al.*[14] also determined parameter sets for C–F and C–Si–F systems based on Brenner's empirical models in order to perform MD simulations of surface reactions caused by fluorocarbon plasmas. Most recently, potential models for Si–O–C–F systems for performing MD simulations of SiO_2 etching by fluorocarbon plasmas were reported by Ohta and Hamaguchi,[15] Ohta,[16] and Smirnov *et al.*[17] The latter is based on SW-type potential functions.[17] In addition, Smirnov *et al.*[18] further extended the SW models to Si–O–C–H systems for plasma etching simulations of low-*k* dielectric materials. Finally, interactions between Ar and other elements can be described by using *Moriére* repulsive pair potentials.[19]

Generally, since halogens show strong chemical reactivity toward Si surfaces, F^+-or Cl^+-containing plasmas have been used for Si etching processes. With the etching process being reduced up to the deep submicron scale, Br^+-containing plasmas such as HBr and Br_2 plasmas have been introduced in the actual manufacturing process. There are several published reports on fundamental experiments on the same.[20–22] On the contrary, no potential models contain-

[a]Present address: Materials Department, University of California, Santa Barbara, CA 93106, USA. Electronic mail: hiroaki.ohta.aug18@gmail.com.

ing Br have been developed, although they are very important in state-of-the-art dry-process techniques.

In this study, we present a procedure for developing a potential model for Si–Br systems based on the well-established SW-type potential. The model parameters are determined entirely from *ab initio* quantum-chemical calculations for small clusters. Herein, we also report a detailed procedure for determining the model parameters and sample simulations of Si etching by a monoenergetic Br^+ beam.

II. SW-TYPE POTENTIAL FUNCTIONS

First, the SW-type potential model for covalent bonds is summarized.[1–3,6] The total energy of an atomic system is expressed by the summation of the two- and three-body potentials as

$$\Phi = \sum_{i<j} v_2(i,j) + \sum_{i<j<k} v_3(i,j,k). \tag{1}$$

The pairlike interaction $v_2(i,j)$ between the ith and the jth atoms takes the following form:

$$v_2(i,j) \equiv v_{ij}(r_{ij}) = A_{ij}(B_{ij}r_{ij}^{-p_{ij}} - 1)\exp\left[\frac{C_{ij}}{r_{ij} - a_{ij}}\right] \quad \text{if} \quad r_{ij} < a_{ij}, \tag{2}$$

and $v_2(i,j)=0$, otherwise. Here, $r_{ij}=|\mathbf{r}_i-\mathbf{r}_j|$ denotes the distance between the ith and jth atoms located at $\mathbf{r}_i$ and $\mathbf{r}_j$. The parameters A_{ij}, B_{ij}, C_{ij}, p_{ij}, and a_{ij} depend on the nature of the ith and jth elements. a_{ij} is the cutoff distance. The system symmetry requires that the parameters become invariant when indices i and j are interchanged, i.e., $A_{ij}=A_{ji}$,….

The three-body term $v_3(i,j,k)$ in Eq. (1) is divided into three parts as

$$v_3(i,j,k) \equiv v_{ijk}(\mathbf{r}_i,\mathbf{r}_j,\mathbf{r}_k) = h_{jik}(r_{ij},r_{ik},\theta_{jik}) + h_{ijk}(r_{ji},r_{jk},\theta_{ijk}) + h_{ikj}(r_{ki},r_{kj},\theta_{ikj}),$$

where θ_{jik} is the angle spanned by $\mathbf{r}_j-\mathbf{r}_i$ and $\mathbf{r}_k-\mathbf{r}_i$. $h_{jik}(r_{ij},r_{ik},\theta_{jik})$ is given by either

$$h_{jik}(r,s,\theta) = \lambda_{jik}\exp\left[\frac{\gamma_{jik}^j}{r-a_{jik}^j} + \frac{\gamma_{jik}^k}{s-a_{jik}^k}\right] \tag{3}$$

or

$$h_{jik}(r,s,\theta) = \lambda_{jik}\exp\left[\frac{\gamma_{jik}^j}{r-a_{jik}^j} + \frac{\gamma_{jik}^k}{s-a_{jik}^k}\right] \times |\cos\theta - \cos\theta_{jik}^0|^{2\alpha_{jik}} \tag{4}$$

depending on the species of the ith atom if $r<a_{jik}^j$ and $s<a_{jik}^k$, otherwise, $h_{jik}=0$. Here, λ_{jik}, γ_{jik}^j, γ_{jik}^k, a_{jik}^j, a_{jik}^k, θ_{jik}^0, and α_{jik} are parameters that depend on the species of the (i,j,k) triplet. a_{jik}^j and a_{jik}^k are the cutoff distances. The system symmetry requires these parameters to be invariant when the first and third indices in the subscripts are exchanged, e.g., $\lambda_{jik}=\lambda_{kij}$, $\gamma_{jik}^j=\gamma_{kij}^j$,…. We have added a new parameter α_{jik} in order to improve parameter fitting to the level achieved in previous studies.[7]

III. PARAMETER FITTING PROCEDURE

A. Quantum-chemical calculations by GAUSSIAN03

Let us introduce two assumptions for the systems studied herein. First, we consider atomic interactions only among charge-neutral species. In other words, isolated clusters such as atoms, molecules, radicals, and the surface itself are maintained neutral. Then, we impose the adiabatic assumption for electron dynamics (Born–Oppenheimer approximation) on the system. Then, the interatomic forces can be obtained from the derivatives of such interatomic potential functions with respect to the position of the nucleus.

For quantum-chemical calculations, we used the general-purpose software "GAUSSIAN03."[23] A density-functional method "B3LYP/6-311+G(d,p)" was adopted as the model chemistry and basis set because our systems contain $_{35}$Br whose atomic number is very high. Although the total charge of the input parameters is always zero since a charge-neutral condition is assumed, the total spin multiplicity S (number of lone pair electrons+1) for each atomic configuration should be specified. The total potential energies calculated for various configurations of small clusters, i.e., the *ab initio* database, were used to determine the interatomic potential functions.

Determination of the parameters involves the following three steps: (1) determination of the two-body functions (v_{BrBr} and v_{SiBr}), (2) determination of the three-body potential given by Eq. (3) (h_{BrBrBr}, h_{BrBrSi}, and h_{SiBrSi}), and (3) determination of the three-body potential given by Eq. (4) (h_{BrSiBr} and h_{BrSiSi}). The energy and length units in our potential functions (parameters) are 50.0 kcal/mol (2.17 eV) and 2.0951 Å, respectively.

B. Two-body functions

First, we determine the parameters for v_{BrBr} and v_{SiBr} for the Br–Br and Si–Br pairs, respectively. The *ab initio* data were obtained from calculations carried out for the Br–Br cluster ($S=1$) and Si–Br cluster ($S=2$) by varying the bond lengths. When the interatomic distance increases, the potential energy values may be overestimated because of the difficulty involved in the accurate calculation of the potential energies for open-shell structures. Hence, we excluded the data that exceeded a reference value.

For the Br–Br pair, the zero reference is considered to be twice the potential energy of an isolated Br atom ($S=2$). Similarly, the zero reference for the Si–Br pair is the sum of potential energies of an isolated Si atom ($S=3$) and a Br atom ($S=2$). The *ab initio* data and potential curves with optimized fitting parameters are shown in Fig. 1. For v_{SiSi}, we use the original SW parameters without further modification.[1] The optimized parameters A_{ij}, B_{ij}, C_{ij}, p_{ij}, and a_{ij} are summarized in Table I. The bond energies and bond lengths calculated by using two-body potential functions are 2.06 eV and 2.34 Å for the Br–Br bond and 3.67 eV and 2.32 Å for the Si–Br bond, respectively (see Table II)

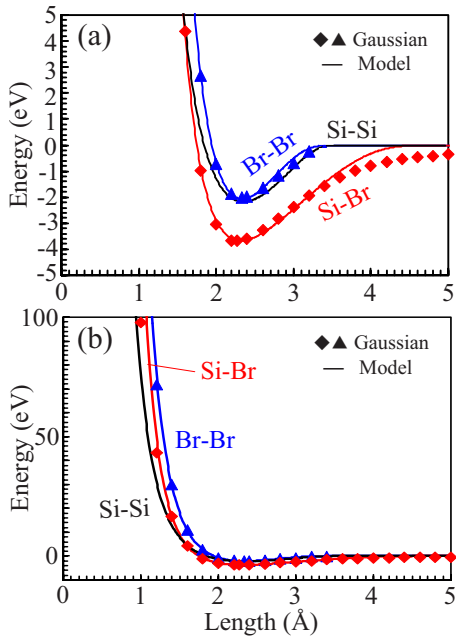

FIG. 1. (Color online) Potential energies for systems containing two atoms.

C. Three-body functions [Eq. (3)]

Next, we determine three-body functions for h_{BrBrBr}, h_{BrBrSi}, and h_{SiBrSi} using the potential function shown in Eq. (3). This function effectively introduces a single valence of a halogen atom by shielding the attractive forces arising from a simple summation of the two-body potentials. Here, we present the method of determination of the fitting parameters for h_{BrBrBr}. The same procedure was applied to the cases of h_{BrBrSi} and h_{SiBrSi}. Note that the two-body potentials determined in the previous subsection are used here.

The function provided by Eq. (3) contains five parameters λ_{jik}, γ^{j}_{jik}, γ^{k}_{jik}, a^{j}_{jik}, and a^{k}_{jik}. On the basis of our preliminary examination (not shown in this paper), we determined

TABLE II. Bond energies and lengths calculated by two-body functions.

	Bond energy (ev)	Bond length (Å)
Si–Si	2.17	2.35
Si–Br	3.67	2.32
Br–Br	2.06	2.34
Si–Cl	3.96	2.06
Cl–Cl	2.47	1.96

γ^{j}_{jik}, γ^{k}_{jik}, a^{j}_{jik}, and a^{k}_{jik} as follows: $\gamma^{j}_{jik}=\gamma^{j}_{kij}=C_{ij}(=C_{ji})$ and $a^{j}_{jik}=a^{j}_{kij}=a_{ij}(=a_{ji})$. As a result, the conditions $\gamma^{\mathrm{Br}}_{\mathrm{BrBrBr}}=C_{\mathrm{BrBr}}$ and $a^{\mathrm{Br}}_{\mathrm{BrBrBr}}=a_{\mathrm{BrBr}}$ were satisfied. The remaining parameter λ_{jik}(in this case, $\lambda_{\mathrm{BrBrBr}}$) should be optimized by considering all the two- and three-body functions for clusters that contain three atoms. The *ab initio* data used here were obtained from the calculations performed for the Br–Br–Br ($S=2$) cluster by varying the bond lengths, with $\theta_{\mathrm{BrBrBr}}=180°$, where the zero reference is thrice the potential energy of an isolated Br atom ($S=2$). Figure 2 shows the two-dimensional potential energy contours calculated using the complete potential model. In this figure, the small numbers indicate the potential energies (eV) corresponding to each contour. The definitions of r_1 and r_2 are provided at the top of the figure. The extracted one-dimensional potential curves are also shown. As shown here, the obtained potential curves are consistent with the *ab initio* data although only λ_{jik} was determined as an independent parameter.

Similarly, the parameters for h_{BrBrSi} and h_{SiBrSi} are determined. Following the abovementioned procedure, we get $\gamma^{\mathrm{Br}}_{\mathrm{BrBrSi}}=C_{\mathrm{BrBr}}$, $a^{\mathrm{Br}}_{\mathrm{BrBrSi}}=a_{\mathrm{BrBr}}$, $\gamma^{\mathrm{Si}}_{\mathrm{BrBrSi}}=C_{\mathrm{SiBr}}$, and $a^{\mathrm{Si}}_{\mathrm{BrBrSi}}=a_{\mathrm{SiBr}}$ for h_{BrBrSi}. We obtained the relations $\gamma^{\mathrm{Si}}_{\mathrm{SiBrSi}}=C_{\mathrm{SiBr}}$ and $a^{\mathrm{Si}}_{\mathrm{SiBrSi}}=a_{\mathrm{SiBr}}$ for h_{SiBrSi}. However, $\lambda_{\mathrm{BrBrSi}}$ and $\lambda_{\mathrm{SiBrSi}}$ were determined separately. The *ab initio* data for the determination of h_{BrBrSi} and h_{SiBrSi} were obtained from the calculations performed for the Br–Br–Si cluster ($S=3$) and Si–Br–Si cluster

TABLE I. Parameter sets for Si–Br systems.

v_{BrBr}	A_{BrBr}	13.65	h_{BrBrBr}	$\lambda_{\mathrm{BrBrBr}}$	83.845	h_{BrSiBr}	$\lambda_{\mathrm{BrSiBr}}$	100.74
[Eq. (2)]	B_{BrBr}	0.7084	[Eq. (3)]	$\gamma^{\mathrm{Br}}_{\mathrm{BrBrBr}}$	1.445	[Eq. (4)]	$\gamma^{\mathrm{Br}}_{\mathrm{BrSiBr}}$	2.749
	C_{BrBr}	1.445		$a^{\mathrm{Br}}_{\mathrm{BrBrBr}}$	1.8		$a^{\mathrm{Br}}_{\mathrm{BrSiBr}}$	2.5
	p_{BrBr}	4.649					$\theta^{0}_{\mathrm{BrSiBr}}$	105
	a_{BrBr}	1.8	h_{BrBrSi}	$\lambda_{\mathrm{BrBrSi}}$	86.650		α_{BrSiBr}	1.3
			[Eq. (3)]					
v_{SiBr}	A_{SiBr}	15.87		$\gamma^{\mathrm{Br}}_{\mathrm{BrBrSi}}$	1.445			
[Eq. (2)]	B_{SiBr}	0.3938		$a^{\mathrm{Br}}_{\mathrm{BrBrSi}}$	1.8	h_{BrSiSi}	$\lambda_{\mathrm{BrSiSi}}$	19.019
	C_{SiBr}	2.749		$\gamma^{\mathrm{Si}}_{\mathrm{BrBrSi}}$	2.749	[Eq. (4)]	$\gamma^{\mathrm{Br}}_{\mathrm{BrSiSi}}$	2.749
	p_{SiBr}	5.186		$a^{\mathrm{Si}}_{\mathrm{BrBrSi}}$	2.5		$a^{\mathrm{Br}}_{\mathrm{BrSiSi}}$	2.5
	a_{SiBr}	2.5					$\gamma^{\mathrm{Si}}_{\mathrm{BrSiSi}}$	1
			h_{SiBrSi}	$\lambda_{\mathrm{SiBrSi}}$	110.82		$a^{\mathrm{Si}}_{\mathrm{BrSiSi}}$	1.8
v_{SiSi}	A_{SiSi}	7.049 556 277	[Eq. (3)]	$\gamma^{\mathrm{Si}}_{\mathrm{SiBrSi}}$	2.749		$\theta^{0}_{\mathrm{BrSiSi}}$	110
[Eq. (2)]	B_{SiSi}	0.602 245 584		$a^{\mathrm{Si}}_{\mathrm{SiBrSi}}$	2.5		α_{BrSiSi}	1
	C_{SiSi}	1						
	p_{SiSi}	4				h_{SiSiSi}	$\lambda_{\mathrm{SiSiSi}}$	16.404
	a_{SiSi}	1.8				[Eq. (4)]	$\gamma^{\mathrm{Si}}_{\mathrm{SiSiSi}}$	1.0473
							$a^{\mathrm{Si}}_{\mathrm{SiSiSi}}$	1.8
							$\theta^{0}_{\mathrm{SiSiSi}}$	109.471 220 6
							α_{SiSiSi}	1

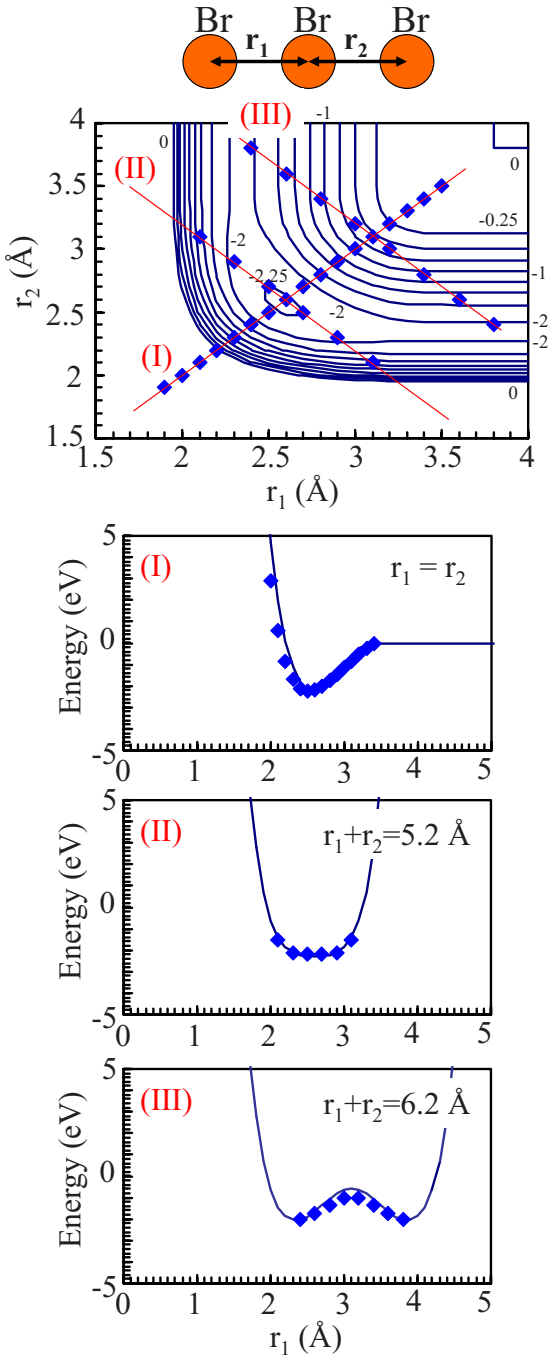

FIG. 2. (Color online) Potential energies for the Br–Br–Br configuration obtained from GAUSSIAN03 (diamonds) and our potential model (solid line).

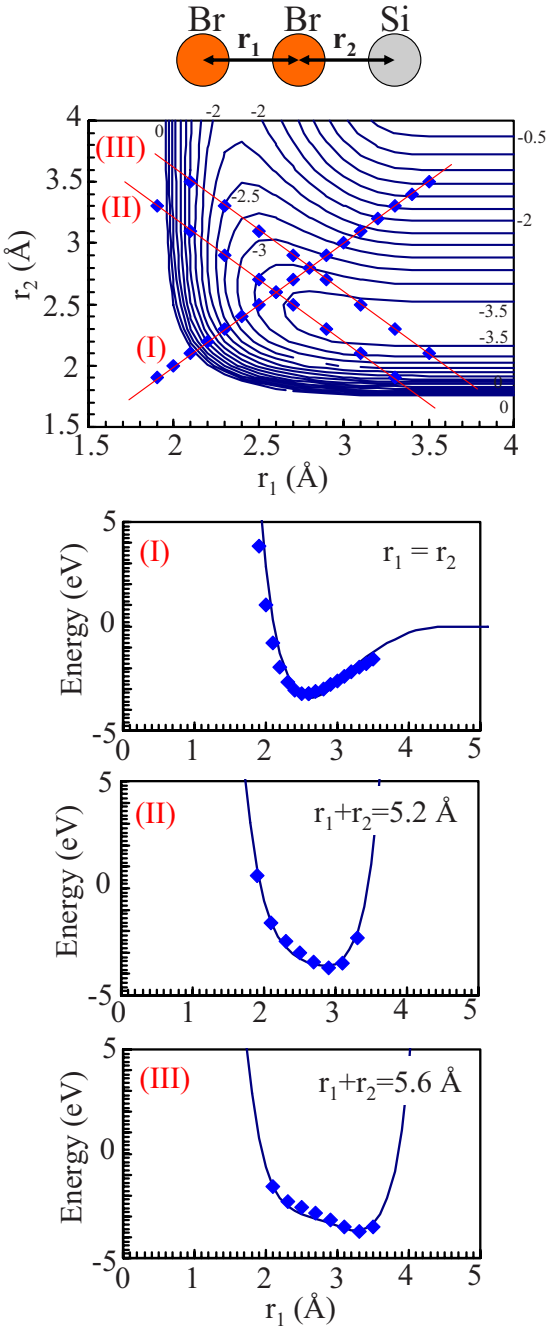

FIG. 3. (Color online) Potential energies for the Br–Br–Si configuration obtained from GAUSSIAN03 (diamonds) and our potential model (solid line).

(S=4), respectively. For these calculations, the bond lengths were used as the scanning parameters, and the three atoms were aligned in a linear fashion. The zero reference values were calculated by the appropriate summation of the potential energies of the Si atom (S=3) and Br atom (S=2). A comparison of the potential energies between GAUSSIAN03 and our model is shown in Figs. 3 and 4. As shown in these figures, our potential functions could reconstruct the *ab initio* data perfectly. Note that this procedure presented here does not require nonlinear fitting, in contrast to that reported in the previous studies;[7] further, only λ_{jik} is considered as the independent parameter. All the parameters determined here are summarized in Table I.

D. Three-body functions [Eq. (4)]

Finally, the parameters for the three-body functions given by Eq. (4) were determined for h_{BrSiBr} and h_{BrSiSi}. For these, we used the conditions mentioned in the previous subsection, i.e., $\gamma^{\mathrm{Br}}_{\mathrm{BrSiBr}}=C_{\mathrm{SiBr}}$, $a^{\mathrm{Br}}_{\mathrm{BrSiBr}}=a_{\mathrm{SiBr}}$, $\gamma^{\mathrm{Br}}_{\mathrm{BrSiSi}}=C_{\mathrm{SiBr}}$, $a^{\mathrm{Br}}_{\mathrm{BrSiSi}}=a_{\mathrm{SiBr}}$, $\gamma^{\mathrm{Si}}_{\mathrm{BrSiSi}}=C_{\mathrm{SiSi}}$, and $a^{\mathrm{Si}}_{\mathrm{BrSiSi}}=a_{\mathrm{SiSi}}$. The remaining parameter sets are ($\lambda_{\mathrm{BrSiBr}}$, $\theta^0_{\mathrm{BrSiBr}}$, α_{BrSiBr}) and ($\lambda_{\mathrm{BrSiSi}}$, $\theta^0_{\mathrm{BrSiSi}}$, α_{BrSiSi}) for h_{BrSiBr} and h_{BrSiSi}, respectively. The parameter sets for h_{BrSiBr} and h_{BrSiSi} were determined separately. We optimized the three parameters simultaneously in order to minimize the errors between the *ab initio* data and our model. The *ab initio* data for the determination of h_{BrSiBr} were obtained from the calculations performed for the Br–

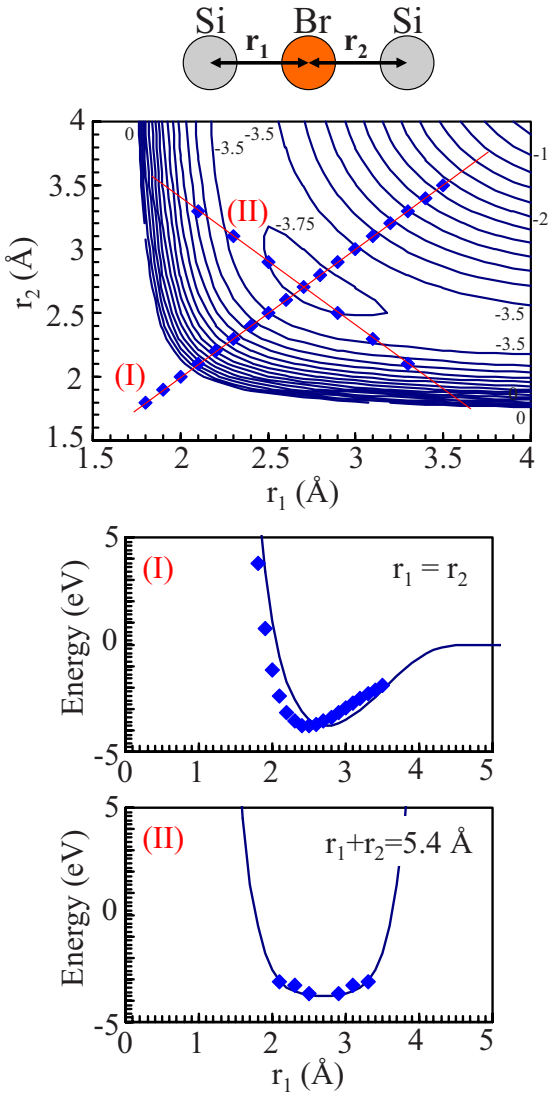

FIG. 4. (Color online) Potential energies for the Si–Br–Si configuration obtained from GAUSSIAN03 (diamonds) and our potential model (solid line).

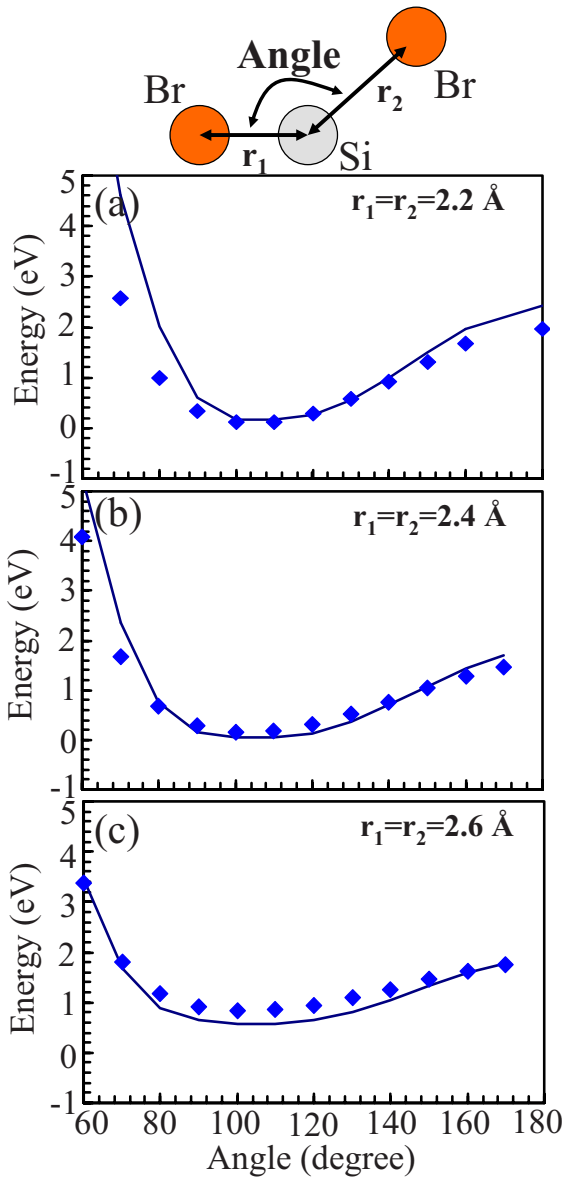

FIG. 5. (Color online) Potential energies for the Br–Si–Br configuration obtained from GAUSSIAN03 (diamonds) and our potential model (solid line).

Si–Br cluster ($S=1$) by varying θ_{BrSiBr} and maintaining the bond lengths constant, where the potential energies for the optimized configuration of $r_1=r_2=2.2833$ Å and $\theta_{\mathrm{BrSiBr}}=103.16°$ were set to be zero as the common reference values for the *ab initio* data and our model. The potential curves with the optimized parameters and the *ab initio* data are shown in Fig. 5. Similarly, the parameters for h_{BrSiSi} were also determined on the basis of the *ab initio* data obtained by scanning θ_{BrSiSi} for the Br–Si–Si cluster ($S=6$). The *ab initio* data and our model for this case are summarized in Fig. 6, where each zero reference for the *ab initio* data and our potential model is the potential energy of the optimized configuration of $r_1=2.2790$, $r_2=2.3817$ Å, and $\theta_{\mathrm{BrSiBr}}=117.64°$. For h_{SiSiSi}, we used the parameters modified by Watanabe *et al.*,[1,6] which are slightly different from the original SW parameters. All the parameters obtained in this study are summarized in Table I.

Potential energies for small stable clusters such as $SiBr_x$ ($x=1-4$) are calculated by using our model and compared with the *ab initio* data by using GAUSSIAN03, as shown in Table III. Since our model does not include the dependency of the two-body functions on the surrounding bond number (i.e., for more than three multibody interactions), the bond energies and bond lengths are almost identical for all the cases. The bond energies in $SiBr_4$ clusters are approximately 15% higher than those obtained from the *ab initio* calculations.

In this study, we determined the parameters on the basis of potential energy data for isolated small clusters. However, the etching characteristics, particularly the spontaneous etching of Si by low-energy (room temperature) particles, should be determined by highly precise potential barriers for ion penetration or absorption on the surface Si atoms. In fact, previous studies have clarified that for more realistic simulation results, and the SW models must be substantially improved.[4,5] Similar discussions for our model for Si/Br systems will be part of our future studies.

IV. TEST SIMULATIONS

Sample MD simulations of Si etching by high-energy Br^+ bombardment were performed by using our potential

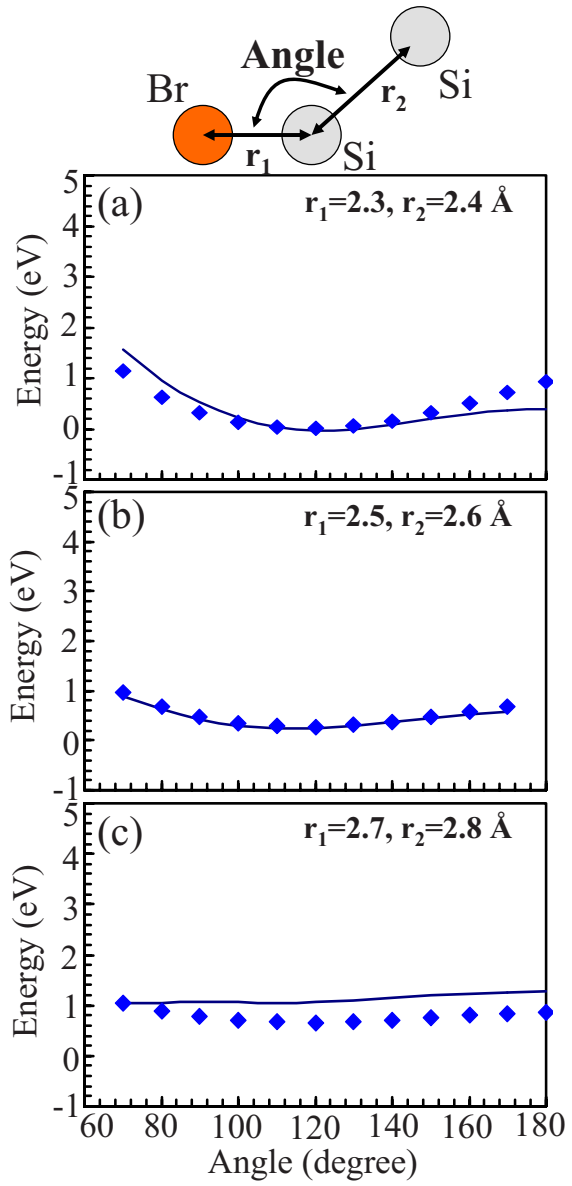

FIG. 6. (Color online) Potential energies for the Br–Si–Si configuration obtained from GAUSSIAN03 (diamonds) and our potential model (solid line).

model. Our simulation technique is summarized briefly in Ref. 24. In the simulations, target atoms are placed in a simulation cell with periodic boundary conditions in the horizontal direction. The Si(100) surface is square shaped with a side length of 32.58 Å (the area is 1061 Å^2) and a monolayer that initially contains 72 Si atoms. Initially, the target contains 20 ML (i.e., 1440 Si atoms), whose depth is 26 Å.

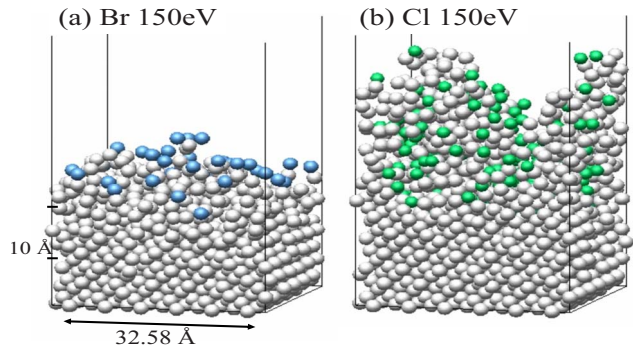

FIG. 7. (Color online) Typical surface structures during etching using 150 eV monoenergetic (a) Br^+ and (b) Cl^+ beams. White, blue, and green spheres indicate Si, Br, and Cl, respectively.

The initial target temperature is 300 K, and the atoms in the bottom layer are rigidly fixed in order to prevent entire simulation cell from drifting.

High-energy atoms are injected from randomly selected horizontal locations immediately above the target in the direction normal to the surface. (Since high-energy ions impinging on the surface are expected to be neutralized near the target surface due to Auger emission, we only consider the charge-neutral atoms as the injected species, i.e., these ions refer to neutral atoms with high translational energy.) Here, the impinging atom is either Br^+ or Cl^+ with a translational energy of 10–150 eV. It is sometimes more convenient to measure the dose of impinging particles in monolayer units, with 1 ML corresponding to 72 impinging particles. After the injection of each atom, we allow the system evolve for 0.7 ps under a constant total energy.[25] For the time integral, the actual mass numbers of ^{28}Si, ^{35}Cl, and ^{80}Br used here are 27.976 929, 34.968 851, and 79.904 000, respectively. We then artificially cool the entire system for 0.3 ps to reduce the temperature of the target to the initial temperature (i.e., 300 K).[26] The target is repeatedly bombarded by a single high-energy particle for approximately 1800 times (approximately 25 ML). Statistically averaged data such as atomic distribution as a function of depth, etching yields, and stoichiometry were obtained by averaging over 15 ML impacts after 10 ML irradiations.

The typical surfaces (after the 10 ML impact) during Si etching by Br^+ and Cl^+ ions with a translational energy of 150 eV are shown in Figs. 7(a) and 7(b), respectively, where the white, blue, and green spheres correspond to Si, Br, and Cl, respectively. Similar to the previous studies, Feil's potential model was adopted for the MD simulation of Si etching by Cl^+.[3,7] The atomic distributions are also shown in Figs.

TABLE III. Si–Br bond energy, Si–Br bond length, and angle spanned by two Si–Br bonds obtained from GAUSSIAN03 and our potential model. *S* indicates the spin multiplicity used in the calculation by GAUSSIAN03.

	Bond energy (ev)		Bond length (Å)		Bond angle (deg)	
	Gaussian	Model	Gaussian	Model	Gaussian	Model
$SiBr(S=2)$	3.68	3.67	2.27	2.32	⋯	⋯
$SiBr_2(S=1)$	3.62	3.67	2.28	2.32	103	105
$SiBr_3(S=2)$	3.09	3.67	2.25	2.32	110	105
$SiBr_4(S=1)$	3.17	3.66	2.22	2.32	109.5	109.5

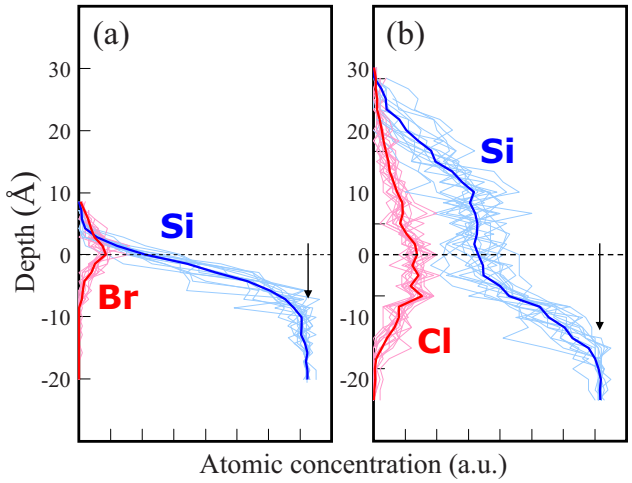

FIG. 8. (Color online) Atomic concentration during etching using 150 eV monoenergetic (a) Br^+ and (b) Cl^+ beams. The arrows correspond to 1 ML (72 atoms for our simulation cell) for the Si diamond lattice. The dashed lines indicate the Si surface defined by the position, where the atomic concentration ratio of Si/Br or Si/Cl is 80%. The thin lines represent the data obtained for every monolayer impact after a steady state (10 ML impact), and the thick lines represent their average.

8(a) and 8(b). Cl atoms can penetrate the Si substrate to a depth of more than 40 Å, as shown in previous studies.[7,27,28] In contrast, Br atoms cannot penetrate the Si lattice and, hence, remain at the vicinity of the surface that leads to relatively flat surface for Br beams compared with Cl beams. As a result, the total halogen coverage (total halogen content in the simulation cell) for the Br impact is smaller than that for the Cl impact. This tendency qualitatively agrees with the results of the experiments performed by Cheng *et al.*[29] using Cl_2/HBr plasmas. Such a difference in the etching characteristics may be essentially caused by the difference in the chemical properties, i.e., potential functions. The details will be published elsewhere.

The Si etching yield and stoichiometry of the etching products $SiBr_x$ and $SiCl_x$ (x=0–4) are summarized as a function of the beam energies in Fig. 9. Si yields (per ion impact) were estimated from the total amount of Si atoms sputtered as etching products: Si_xBr_y and Si_xCl_y ($x \geq 1$, $y \geq 0$). During beam etching, the halogen flux into the simulation cell equals the total halogen content in the etching products, i.e., both these values are equal to 1 (per impact) after the etching characteristics are statistically stabilized. The estimated Si yield for the Br^+ bombardment is smaller than that for the Cl^+ beam bombardment at the same incident energy. This tendency is in good agreement with the experimental results published in Refs. 20 and 21. Using mass-selected reactive ion beam etching systems, Tachi *et al.*[20] reported that the etching yield for the Br^+ beam is lower than that for the Cl^+ beam in the energy range of 100–3000. Vitale *et al.*[21] also showed that the Si yields obtained with Cl_2 plasma are higher than those obtained with Br_2 plasmas. Note that the flux ratio of radicals to ions is in the order of 10^3 in Ref. 21. At a low energy (less than 50 eV), the total Si yields obtained are almost the same. The threshold energies for the Br^+ and Cl^+ beams were almost the same in our simulation. It is probably because of the similarity in the chemical characteristics of Br and Cl, as shown in Table II. As shown in Fig. 9(b), Si-containing etch products contained more halogen atoms per Si atom when Br^+ beams are used. This is partially caused by the high concentration of Br (high Br/Si ratio) near the surface [see Figs. 7(a) and 8(a)]. The use of the Cl^+ beam afforded a large amount of Si and SiCl products. It is considered that Si is sputtered more physically because of the roughness of the surface (i.e., microscopically off-angle beam injection to surface atoms). Further discussions, particularly, the relation between potential barriers for ion penetration and the simulation results, have been reported by Iwakawa *et al.*[31]

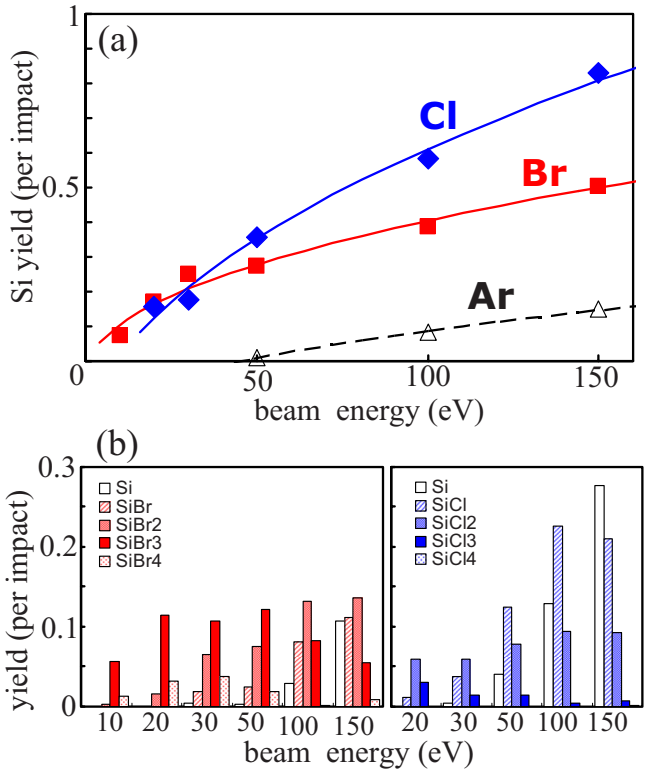

FIG. 9. (Color online) (a) Si etching yields per impact and (b) their stoichiometry during Si etching by Br^+ and Cl^+ beams. The Si yields obtained by using monoenergetic Ar beams are shown in Ref. 24. Note that these yields were obtained by averaging the data after the steady state (10 ML impact). The fitting curves $\propto \sqrt{\text{beam energy}} - \sqrt{E_{th}}$ are also shown in (a) (Refs. 24 and 30).

V. SUMMARY

In summary, we have developed a potential model for Si–Br systems to perform classical MD simulations. Our potential model is based on the well-known SW model, while the parameters are determined from the data for small clusters containing up to three atoms. This model enables us to simulate Si etching by Br^+-containing plasmas. The preliminary simulation results of Si etching by monoenergetic Br^+ beams qualitatively agreed with the experimental results. This simple systematic procedure for constructing parameters can be easily applied to other unexplored systems.

ACKNOWLEDGMENTS

This study was partially supported by the 21st Century COE Program "Center of Excellence for Research and Education on Complex Functional Mechanical Systems."

[1]F. H. Stillinger and T. A. Weber, Phys. Rev. B **31**, 5262 (1985); J. Chem. Phys. **88**, 5123 (1988); Phys. Rev. Lett. **62**, 2144 (1989).
[2]T. A. Weber and F. H. Stillinger, J. Chem. Phys. **92**, 6239 (1990).
[3]H. Feil, J. Dieleman, and B. J. Garrison, J. Appl. Phys. **74**, 1303 (1993).
[4]P. C. Weakliem, C. J. Wu, and E. A. Carter, Phys. Rev. Lett. **69**, 200 (1992).
[5]D. E. Hanson, A. F. Voter, and J. D. Kress, J. Chem. Phys. **110**, 5983 (1999).
[6]H. Ohta and S. Hamaguchi, J. Chem. Phys. **115**, 6679 (2001).
[7]T. Watanabe, H. Fujiwara, H. Noguchi, T. Hosino, and I. Ohdomari, Jpn. J. Appl. Phys., Part 2 **38**, L366 (1999).
[8]J. Tersoff, Phys. Rev. Lett. **56**, 632 (1986); Phys. Rev. B **37**, 6991 (1988); **38**, 9902 (1988).
[9]J. Tersoff, Phys. Rev. Lett. **61**, 2879 (1988).
[10]J. Tersoff, Phys. Rev. B **39**, 5566 (1989).
[11]D. W. Brenner, Phys. Rev. B **42**, 9458 (1990).
[12]D. W. Brenner, O. A. Shenderoval, J. A. Harrison, S. J. Stuart, B. Ni, and S. B. Sinnott, J. Phys.: Condens. Matter **14**, 783 (2002).
[13]J. Tanaka, C. F. Abrams, and D. B. Graves, J. Vac. Sci. Technol. A **18**, 938 (2000).
[14]C. F. Abrams and D. B. Graves, J. Vac. Sci. Technol. A **16**, 3006 (1998).
[15]H. Ohta and S. Hamaguchi, J. Plasma Fusion Res. **6**, 399 (2004).
[16]H. Ohta, Ph.D. thesis, Kyoto University, 2004.
[17]V. V. Smirnov, A. V. Stengach, K. G. Gaynullin, V. A. Pavlovsky, S. Rauf, P. J. Stout, and P. L. G. Ventzek, J. Appl. Phys. **97**, 093302 (2005).
[18]V. V. Smirnov, A. V. Stengach, K. G. Gaynullin, V. A. Pavlovsky, S. Rauf, and P. L. G. Ventzek, J. Appl. Phys. **101**, 053307 (2007).
[19]I. Torrens, *Interatomic Potentials* (Academic, New York, 1972).
[20]S. Tachi and S. Okudaira, J. Vac. Sci. Technol. B **4**, 459 (1986).
[21]S. A. Vitale, H. Chae, and H. H. Sawin, J. Vac. Sci. Technol. A **19**, 2197 (2001).
[22]W. Jin, S. A. Vitale, and H. H. Sawin, J. Vac. Sci. Technol. A **20**, 2106 (2002).
[23]M. J. Frisch, G. W. Trucks, H. B. Schlegel *et al.*, Gaussian, Inc., Pittsburgh PA, 2003.
[24]H. Ohta and S. Hamaguchi, J. Vac. Sci. Technol. A **19**, 2373 (2001).
[25]R. Smith and D. E. Harrison, Jr., Comput. Phys. **3**, 68 (1989).
[26]H. J. C. Berendsen, J. P. M. Postma, W. F. van Gunsteren, A. DiNola, and J. R. Haak, J. Chem. Phys. **81**, 3684 (1984).
[27]M. E. Barone and D. B. Graves, Plasma Sources Sci. Technol. **5**, 187 (1996).
[28]D. E. Hanson, A. F. Voter, and J. D. Kress, J. Appl. Phys. **82**, 3552 (1997).
[29]C. C. Cheng, K. V. Guinn, I. P. Herman, and V. M. Donnelly, J. Vac. Sci. Technol. A **13**, 1970 (1995).
[30]C. Steinbrüchel, Appl. Phys. Lett. **55**, 1960 (1989).
[31]A. Iwakawa, H. Ohta, K. Eriguchi, and K. Ono, Jpn. J. Appl. Phys. **47**, 6464 (2008).